Experimental investigation of particle heating in a strongly coupled dusty plasma

R. A. Quinn and J. Goree[a)]

Department of Physics and Astronomy, The University of Iowa, Iowa City, Iowa 52242

Highly charged dust particles in a plasma can be strongly coupled when their kinetic temperature is low. This temperature is determined by a balance of heating and gas cooling. The heating is believed to be electrostatic, although its exact nature is still under investigation. Experiments in a multiple-layer plasma crystal were conducted to test proposed heating mechanisms. A method for measuring small-amplitude, low-frequency fluctuations in ion density was developed and, using this, very low-frequency electrostatic fluctuations were found upstream of the particles. These fluctuations should propagate with the ions towards the particles and heat them. However, the fluctuations were uncorrelated with, and too weak to account for, the observed particle temperatures. In the experiment, the temperature increased and then decreased with gas pressure; this result is only partly consistent with an ion wake heating mechanism. These negative findings help narrow the range of possible explanations for the observed temperatures. © *2000 American Institute of Physics.* [S1070-664X(00)01109-5]

I. INTRODUCTION

Laboratory dusty plasmas are useful for studying plasma–dust interactions, strongly coupled plasmas, Coulomb lattices, and phase transitions. They typically consist of a low-density cloud of micron-sized particles embedded in a background of ions and electrons. The particles (dust) are highly negatively charged, and they interact through a strong Coulomb repulsion. The background ions and electrons supply the charge to the dust grains and partially screen the interparticle repulsion. Since the particles are easily imaged using a video camera and laser light scattering, detailed studies of the microstructure and dynamics of the particle cloud can be conducted.

Many recent dusty plasma experiments have focused on a solidlike strongly coupled Coulomb state called a plasma crystal.[1–5] In these experiments, the particles are levitated in the vertical direction by a deep potential well formed by the sheath electric field and gravity, and are confined by a weak radial electric field. The particle kinetic energy is reduced so much by collisions with neutral gas molecules that the Coulomb repulsion between particles leads to highly-ordered arrangements of the particles in a crystal-like Coulomb lattice. These experimental strongly-coupled plasmas are valuable because most previous strong-coupling research was theoretical.[6–8]

A measure of the expected amount of order in a plasma crystal is given by the Coulomb coupling parameter, $\Gamma = Q_0^2/\Delta T \exp(-\kappa)$. The parameter Γ is the ratio of interparticle potential energy to particle kinetic energy where Q_0 is the mean charge, Δ is the mean nearest neighbor distance,[9] T is the kinetic temperature of the particles, $\kappa = \Delta/\lambda_D$, and λ_D is the Debye screening length due to the plasma. In general,

strongly-coupled plasmas have $\Gamma > 1$, with more highly ordered phases having progressively larger values of Γ. A variation in any of Q_0, Δ, T, or κ could, in principle, drive a phase transition in the plasma crystal.

Plasma crystals do exhibit phase transitions from solid to liquid or gas when discharge conditions are varied by changing the neutral gas pressure or rf power.[10–12] However, computing Γ for these experiments is difficult,[10,13] and the degree of order (or phase) is usually determined by calculating the translational correlation length and other order parameters based on the relative positions of the particles.[14–16] Nevertheless, the results of Melzer *et al.*[10] and Thomas *et al.*[11] show that the particle kinetic temperature increases as the Coulomb lattice becomes more disordered, while Q_0 and Δ remain approximately constant.[10] (The parameter κ is even more difficult to determine in a plasma crystal melting experiment, but is thought to remain approximately constant.)

As the above discussion illustrates, the particle temperature plays a significant role in determining the structure and dynamics of laboratory dusty plasmas. Therefore, an interesting question to ask is: what controls or determines the particle kinetic temperature? In this paper we report an experiment that answers this question, in part.

Specifically, we are interested in the kinetic particle temperature T associated with the random motion of the whole particle. We use the term ''kinetic'' to avoid confusion with the surface temperature of the particle, which can be entirely different. To measure the kinetic temperature, experimenters and simulators commonly measure particle velocities and compute

$$T_{ms} = m\langle (v - \langle v \rangle)^2 \rangle, \tag{1}$$

where m is the particle mass, v is a single vector component of the particle velocity, and the brackets denote averages over many individual particle velocities. The particle drift

velocity $\langle v \rangle$ is subtracted in computing the temperature. Here the subscript ''ms'' denotes ''measured from the mean-square velocity,'' to distinguish it from the true value, T.

The measured temperature T_{ms} may overestimate the true temperature T for several reasons. First, the drift velocity may vary in time, making $\langle v \rangle$ difficult to compute accurately. Second, long-wavelength coherent particle oscillations enter into Eq. (1), even though they do not represent random thermal motions. As far as we know, there has been no attempt to account for these two problems in previous experiments. For this reason it is unclear how closely T_{ms} approximates the true kinetic temperature, but it is likely to be strongly correlated. We discuss this issue further in Appendix B.

The true particle kinetic temperature T is determined by a balance between particle heating and cooling. Cooling is thought to be primarily due to neutral gas drag,[17,18] which is proportional to the gas density. However, this linear relationship by itself does not account for the variation of T_{ms} with neutral gas pressure which we report in Sec. IV. Brownian collisions with the neutral gas should heat the particles to room temperature, $\approx 1/40$ eV, but this is insufficient to explain the large ~ 10 eV or higher particle kinetic temperatures reported here, and in some other experiments.[10,11,13] Hence an alternative heating mechanism is sought.

Fluctuating electrostatic fields in the plasma could heat the particles, as has been suggested previously.[19–21] To raise the kinetic temperature, these fluctuations would need several properties. First, only fluctuations with frequencies near the dust plasma frequency $\omega_p = (4\pi n_p Z^2 e^2/m)^{1/2}$ can significantly move the particles.[21] Here $Z = |Q_0/e|$ is the average charge number on the particles, and n_p is their number density. For typical plasma crystal experiments, $\omega_p/2\pi \sim 10$ Hz.[13] Second, the fluctuations must have short wavelengths to move nearest neighbors differentially and thus create incoherent particle motions. Third, they must be present where the particles are located. For ground-based plasma crystal experiments in rf discharges, this means the fluctuations must be present inside the sheath where the particles are levitated by the strong electric force.

The fluctuations might originate within the sheath, perhaps driven by ions streaming past the particles.[22–24] Alternatively, they might originate further upstream, in the main plasma, and then propagate with the ion flow into the sheath. Such fluctuations at frequencies as low as 10 Hz are present in a rf plasma, as we will show experimentally, although they have only been mentioned in the rf gas discharge literature in the context of eliminating them from probe measurements. The origin of these fluctuations is undetermined; however, the low frequency, far below the ion plasma frequency, suggests that they might be due to disturbances in the ionization balance.

Particles could also be heated by the interaction of their random charge fluctuations with the levitating dc electric field in the sheath. Random charge fluctuations have been predicted to occur for any particle immersed in a plasma.[25–27] The spectrum of these fluctuations has been predicted to have a significant low-frequency component.[25] A fluctuation in a particle's charge creates a fluctuation in the electric force that levitates the particle. The fluctuating force can in turn lead to random particle motions, thus heating the particle. This heating mechanism is explored in Refs. 21 and 28.

Here, we report an experiment in an rf dusty plasma to determine whether particles are heated by low frequency electrostatic fluctuations in the sheath electric field. To do this, we measure electrostatic fluctuations generated upstream of the particles. We find that such fluctuations are present but are uncorrelated with T_{ms}, indicating that they do not heat the particles. This conclusion is also supported by a separate analysis of the fluctuation levels, along with estimates of the particle charge from the T_e measurements described below, which yielded a predicted temperature much lower than T_{ms}.[21] This information is useful in narrowing the field of candidate particle heating mechanisms.

II. EXPERIMENTAL SETUP

Experimental tests were carried out to measure electrostatic fluctuation levels in a dusty plasma and compare these to measurements of T_{ms}. The experiment was conducted using a plasma crystal formed by particles levitated in the dc sheath of an asymmetric rf discharge. In previous experiments using similar apparatus, the particle temperature was varied by changing either the rf power or the neutral gas pressure.[2,10–12] Following this example, we chose to vary the pressure. The structure and phase of the plasma crystal were also determined, using the method and criteria of Ref. 14.

Highly charged plastic microspheres were levitated by the strong electric field in the dc sheath of a rf discharge plasma. Particle dynamics were studied using laser-light scattering and video imaging under various discharge conditions. The particles were 9.4 ± 0.3 μm diameter, with a mass density of 1.51 g/cm^3. After insertion into the plasma, several thousand particles were found to be arranged in a cloud of two to three vertically aligned layers above a horizontal electrode. A schematic diagram of the experimental system is shown in Fig. 1.

The discharge was formed in a Gaseous Electronics Conference (GEC) Reference Cell, which was modified as described in Ref. 15. The plasma was sustained using a rf amplifier operated at 13.55 MHz, which was capacitively coupled to the electrode through a matching network. The discharge conditions were varied by changing the Krypton neutral gas pressure from 55 to 200 mTorr while fixing the peak to peak electrode voltage at 85 ± 2 V. The dc bias voltage varied from -25 V to -18 V over this pressure range.

Particle measurements were made using laser light scattering and video imaging. A slice of the particle cloud was illuminated with two HeNe laser sheets, one horizontal and the other vertical, and the scattered light was recorded on a SVHS video cassette recorder (VCR) using a charge-coupled device (CCD) camera fitted with either a Nikon macro lens or a long-distance microscope, as shown in Fig. 1(a). The camera shutter speed was 1/250 s. Particle locations were identified by first digitizing a sequence of images from the recorded video. Up to 32 consecutive frames of video were digitized at the video rate of 30 frames per second and re-
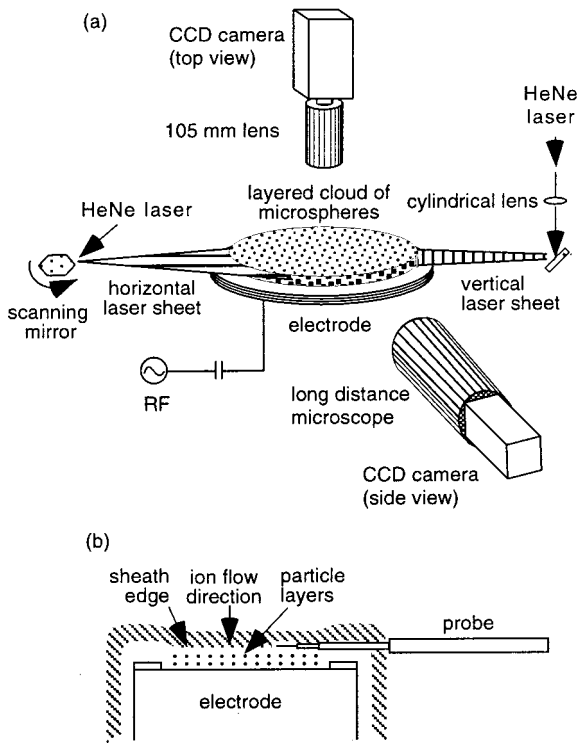
FIG. 1. Perspective view of electrode and particle imaging. (a) A 13.55 MHz rf voltage is applied between the electrode and the vacuum chamber (not shown). Charged particles are levitated in the sheath above the electrode. Horizontal and vertical laser sheets illuminate the particles and video cameras record their trajectories. (b) Side view sketch of the electrode, particles, visible sheath edge, and Langmuir probe. The probe is used to measure ion density fluctuations upstream of the particles.

FIG. 2. (a) Probe assembly. (b) Amplifier circuit. Noise reduction features include batteries to power the amplifier and bias the probe, differential detection, and filters.

corded as 640×480 bit-mapped images. Each 480-line frame consisted of two interleaved fields separated in time by 1/60 s. Splitting the fields allowed a temporal resolution of 1/60 s for a spatial field of 640×240 pixels. After thresholding each image to identify the particles, we recorded the two-dimensional (2D) coordinates of the particle centers.

III. MEASUREMENT TECHNIQUES

A. Fluctuation measurements

We expect the measured temperature T_{ms} to increase with the ion density fluctuation level $\delta n_i/n_i$, if electrostatic fluctuations dominate the particle heating. A Langmuir probe operated at ion saturation was used to measure $\delta n_i/n_i$ at the sheath edge, as described below, and in Appendix C. The ion saturation current is $I_{sat} \propto n_i T_e^{1/2}$, where $T_e^{1/2}$ usually varies much less than n_i in most discharges. Therefore $\delta n_i/n_i \approx \delta I_{sat}/I_{sat}$, where n_i and I_{sat} are the mean ion density and saturation current, respectively.

An rf-compensated Langmuir probe was used to measure the ion saturation current just above the visible sheath edge. The probe, shown in Fig. 1(b), was located upstream of the particles, which were levitated within the sheath. The probe design, shown in Fig. 2(a), was based on suggestions of Godyak[29] and Overzet. The tip measured 5 mm long and 0.075 mm diam. A coaxial reference probe of 10 mm length and 1.8 mm outside diameter was coupled to the probe tip

through a 50 pF capacitor. Three choke inductors blocked rf at 13, 26, and 40 MHz. To measure the ion saturation current, a bias voltage of -27 V was applied to the probe. While fluctuations with a characteristic wavelength shorter than the length of the probe tip may have been attenuated, this was not thought to be a significant problem since only waves propagating within a small solid angle about the probe tip axis would be affected. All other waves would cross the tip's much smaller diameter.

The ion saturation current power spectrum $G_i(\omega) \equiv \delta I_{sat}/I_{sat}$ was measured by biasing the probe to -27 V, measuring the ac (δI_{sat}) and dc (I_{sat}) components of the probe current, and taking fast Fourier transforms (FFTs). The measurement required the use of a small-current sensor-amplifier, shown in Fig. 2(b), as well as measures to reduce 60 Hz noise contamination. Further details of the measurement are given in Appendix C.

The normalized root-mean-square (rms) ion density fluctuation δn_{rms} was computed from the single-sided power spectrum, $G_i(\omega)$. Recall that $\delta n_i/n_i \approx \delta I_{sat}/I_{sat}$, so that

$$\delta n_{rms} = \left(\int_0^{BW} G_i(\omega) \frac{d\omega}{2\pi} \right)^{1/2}. \tag{2}$$

Equation (2) was computed numerically by integrating the measured $G_i(\omega)$ FFT power spectrum over a bandwidth BW =1000 Hz. Additionally, we verified that the particle layer

downstream of the probe was not the cause of the measured fluctuations by repeating the fluctuation measurements without particles present in the plasma.

B. Electron temperature measurements

Since, according to Ref. 21, T_{ms} is expected to be proportional to Q_0^2, the Langmuir probe was also used to measure the electron temperature, T_e. The particle charge number is $Q_0/e \equiv Z = K_Q a T_e$, where a is the particle radius and K_Q is a numerical coefficient which must be computed using the orbital-motion-limited (OML) charging model.[30] (See Ref. 21 for K_Q, tabulated for various plasma parameter values.) Here, the electron temperature was measured at the sheath edge and in the main plasma region. The probe voltage was stepped in 0.25 V increments from -20 V to $+30$ V while recording the current. After subtracting the ion saturation contribution, a fit to the exponential portion of each current–voltage ($I–V$) curve yielded T_e. This was repeated for 11 neutral gas pressures between 55 and 200 mTorr. To estimate error bars, measurements were repeated three times, 15 min apart, at five of the pressures.

C. Particle kinetic temperature measurements

Particle trajectories in a vertical slice of the dust cloud were obtained using a long-distance microscope. The field of view was approximately 1.3×1.0 mm, which yielded a spatial resolution of ~ 2.0 μm per pixel. The interparticle spacing was ~ 500 μm, so that 1–4 particles were in the field of view at any time. Because a vertical slice of the cloud was viewed, two components of the particle trajectories were observed; a vertical component denoted by (z) and a horizontal component denoted by (x,y). The designation (x,y) is used since the temperature is assumed to be isotropic in the horizontal plane. Particles in two of the three layers were typically imaged.

Trajectories of individual particles were obtained as follows. Video was digitized to yield the coordinates of all the particles in a single field. This was repeated for 10 separate blocks, each consisting of 64 consecutive fields. The trajectories were found using a computer algorithm that ''threaded'' a particle in one field to the same particle in the next. The algorithm started with a particle P1 in a field and searched for the closest particle P2 in the next consecutive field. Particle P2 was considered threaded (matched) to P1 when the separation distance between P1 and P2 was less than the minimum interparticle separation calculated using all of the fields in the block.

Particle velocities were calculated along each step i of each particle trajectory using $v_{\alpha,i} = \Delta D_{\alpha,i}/\Delta t$. Here $v_{\alpha,i}$ is a vector component of the ith particle velocity, $\Delta D_{\alpha,i}$ is the component of the corresponding particle displacement during the time step $\Delta t (= 1/60$ s) between fields, and $\alpha = (x,y)$ or (z) indicates the horizontal or vertical vector component, respectively.

The velocity distributions were found to be approximately Maxwellian, with different temperatures $T_{ms}^{(x,y)}$ and $T_{ms}^{(z)}$ in the horizontal and vertical directions. Equation (1) was used to calculate the two components of T_{ms} from all the
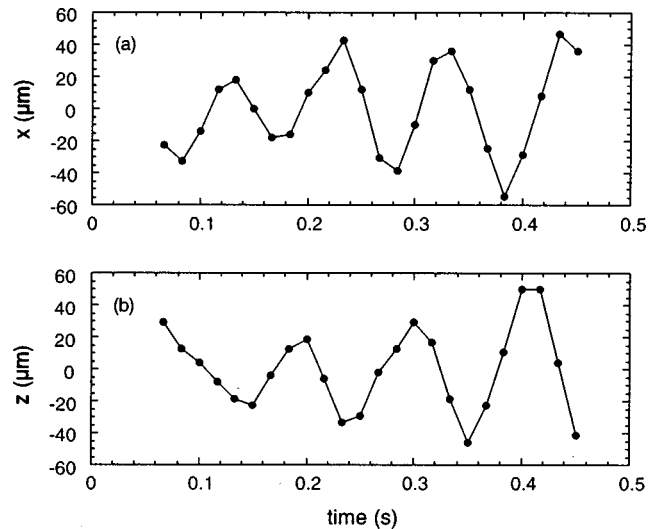
FIG. 3. Particle trajectory recorded using side-view camera. This trajectory, recorded at 60 mTorr, was one of the few long trajectories recorded. The (a) horizontal $x(t)$ and (b) vertical $z(t)$ components of the particle trajectory are shown.

individual particle velocities $v_{\alpha,i}$. This procedure makes no distinction between correlated and random particle motion, an issue we now address.

The true particle kinetic temperature T is the kinetic energy associated with random, uncorrelated particle motions. It should not include the kinetic energy associated with directed particle flows[10–12] or long-wavelength particle oscillations,[31,32] which are predicted to occur in laboratory dusty plasmas. The problems associated with computing a good estimate (T_{ms}) for T from experimental data are discussed in detail in Appendix B, and a solution is suggested.

Here, we simply note that one of our measured single-particle trajectories does show evidence of oscillatory behavior. The x and z components of this trajectory are shown in Fig. 3 for the short time interval in which we were able to track the particle. This trajectory is unusually long for our experiment; most particles could only be tracked for a fraction of a second. We also note that Fig. 3 resembles a circular particle orbit, similar to those found by Melandsø[33] in a three-dimensional (3D) plasma crystal simulation. It is unknown whether this type of trajectory is representative for our experiment, because no other orbits we recorded stayed in the laser sheet as long as this one.

D. Structural measurements

Measures of structural order in the plasma crystal were obtained by computing the translational correlation length and sixfold coordination fraction from particle positions in a horizontal slice of the particle cloud. The particle images used in this computation contained about 100–200 particles. After obtaining the (x,y) coordinates of the particles in each frame, the structural analysis was performed as discussed in Refs. 14–16. The pair correlation function was computed directly from the measured particle coordinates and averaged over 30 frames digitized from video every 0.5 s. The translational correlation length is the scale length for the expo-

nential decay of this function. We also computed the sixfold coordination fraction by dividing the number of particles in a frame having six nearest neighbors by the total number of particles in the frame, and averaging over 30 frames.

IV. RESULTS

While we did measure finite values of the rms ion density fluctuations δn_{rms}, we found no correlation between δn_{rms} and the measured particle temperature T_{ms}. This indicates that electrostatic fluctuations near the sheath edge do not account for the particle heating downstream. The lack of correlation is illustrated in Fig. 4, which show ion density fluctuations, T_e, T_{ms}, and degree of structural order as functions of neutral gas pressure, and in Fig. 5, which shows plots of δn_{rms} vs $T_{ms}^{x,y}$ and translational scale length.

The ion density fluctuation was small, typically 0.005 of the average ion density, as shown in Fig. 4(a). More importantly, this fractional ion density fluctuation varied by only about 50% over the measured pressure range. Over the same pressure range, however, T_{ms} varied by nearly an order of magnitude, first increasing and then decreasing with increasing neutral gas pressure as shown in Fig. 4(c). Measures of structural order in Fig. 4(d) varied by a factor of 2–3, over the pressure range we tested, and they were inversely related to T_{ms}, as expected.

In the main plasma region, our Langmuir probe measurements indicated a two-temperature electron distribution. This is different from the Druyvesteyn distribution that is often observed at higher gas pressures.[29] As shown in Fig. 4(b), the temperature of the hot electron component varied slightly, by 10%, over the measured pressure range. The cold electron component had a temperature similar to that measured near the sheath edge, where a single temperature distribution was observed.

V. CONCLUSION

We find that low-frequency electrostatic fluctuations created upstream, and then propagating toward the particles in the sheath, do not account for the measured particle temperature T_{ms}. This conclusion is supported by the fact that T_{ms} was not correlated with the upstream fluctuations. Further, the fluctuations were of such a small amplitude that the corresponding particle temperature predicted by a Langevin model,[21] is several orders of magnitude smaller than T_{ms}. The negative outcome of the test of our hypothesis is useful since it helps narrow the range of possible particle heating mechanisms. In particular, if particles are heated solely by electrostatic fluctuations, then these fluctuations must originate downstream of the sheath edge, near the particles.

An alternative heating mechanism, involving fluctuations that originate in the particle layer itself, has been proposed.[23,24,33] In this mechanism, particle motions in a lower layer of a multilayer plasma crystal become unstable due to an attractive force between the layers. The attractive force exists because of enhanced ion density in a wake below the upper layer. This instability is predicted to be strengthened when the gas pressure decreases, which is consistent
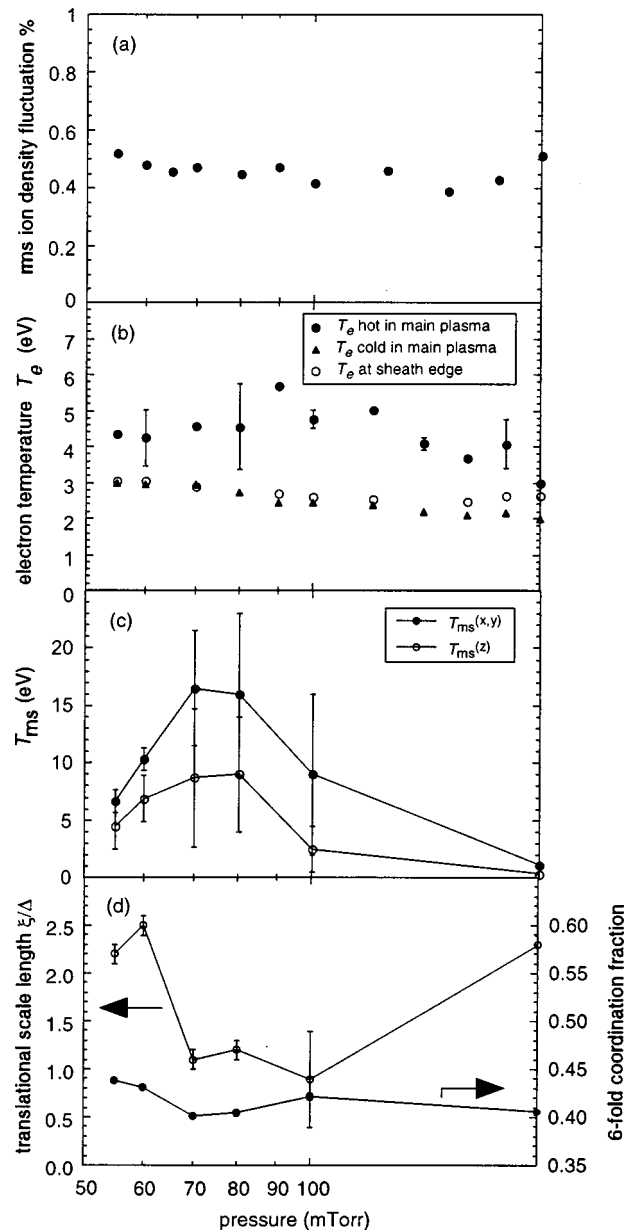
FIG. 4. Measurements as a function of neutral gas pressure. (a) Root-mean-square ion density fluctuation δn_{rms} upstream of the particles, computed from the measured fluctuation spectrum using Eq. (2) with a bandwidth of 1000 Hz, as a percentage of the average ion density. (b) Electron temperature. The electron energy distribution was found to be characterized by a single temperature near the sheath edge and by two temperatures in the main plasma region. Error bars based on multiple measurements, separated in time, are on the order of the symbol size, except for the high T_e component of the main plasma, for which five representative error bars are shown. (c) Measured particle kinetic temperature for motion parallel $T_{ms}^{(x,y)}$ and perpendicular $T_{ms}^{(z)}$ to the horizontal electrode. The lack of correlation of this temperature with the fluctuation levels shown in panel (a) indicates that electrostatic fluctuations in the region upstream of the sheath edge do not account for the particle heating. (d) Translational correlation length and sixfold coordination fraction. Larger values indicate a more highly ordered structure. Comparison with (c) indicates that the structural order is low when the particle kinetic temperature is high, as expected.

with our results in Fig. 4(c) for pressures greater than 80 mTorr, but not consistent with our results for pressures less than 80 mTorr.

Several alternative heating mechanisms have been pro-
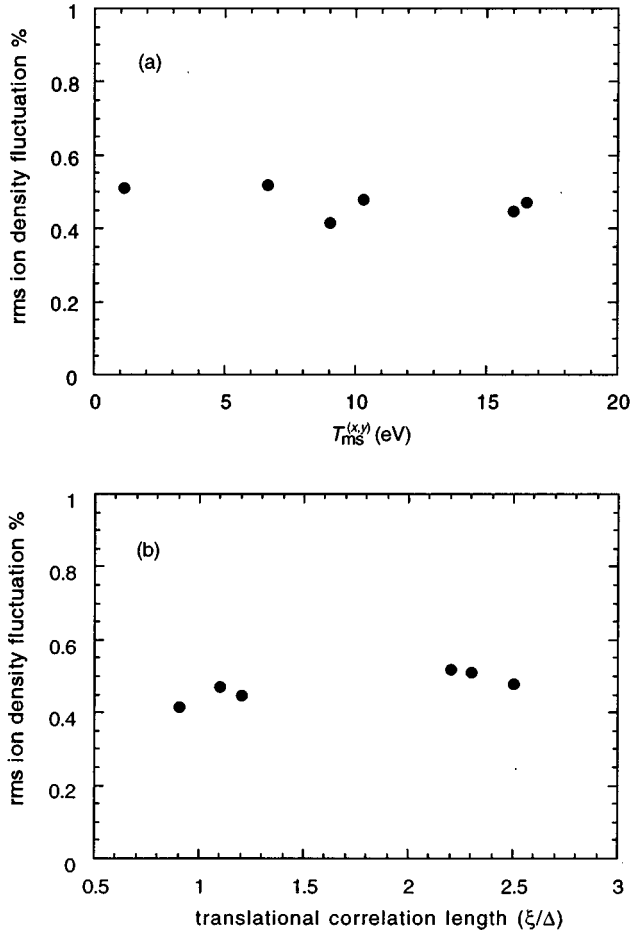
FIG. 5. Ion density fluctuations upstream of the particles, as a percentage of the average ion density. These data are from Fig. 4, replotted so that the horizontal axis is (a) effective particle temperature (in the horizontal direction) and (b) translational scale length. The lack of correlation between δn_{rms} and both T_{ms} and the translational correlation length suggests that these fluctuations are not responsible for heating the particles.

posed that involve charge fluctuations. In one class of these mechanisms, random charge fluctuations due to the stepwise collection of ions and electrons drives random particle motion in the presence of the dc sheath electric field.[21,28] Another heating mechanism has been proposed by Zhakhovskii et al.[34] This mechanism involves charge fluctuations due to a variation in charge with position in the dc electric field region of a standing striation. Because of the positional dependence of the charge and the levitating potential, the interparticle force is not derivable from the gradient of a potential, and it therefore represents a free energy source capable of heating the particles. A variation of this heating mechanism proposed by Nunomura et al.,[35] involves an instability due to the finite charging time. In Nunomura's instability, the actual charge is out of phase with the local equilibrium charge.

APPENDIX A: INTERPARTICLE SPACING, DENSITY, AND PLASMA PARAMETERS

The characteristic particle separation b for a system of particles can be defined in several possible ways. The definition generally depends on the dimensionality of the system and the particle arrangement. For lattice structures, the usual choice is $b = \Delta$, the nearest-neighbor distance, which is also the lattice constant. For square (2D) and cubic (3D) lattices, $\Delta_s = \sqrt{1/n_{2D}}$ and $\Delta_c = \sqrt[3]{1/n_{3D}}$, where n_{2D} and n_{3D} are the 2D and 3D particle densities, respectively. For other lattice types, it is convenient to express the Δ for that lattice in terms of Δ_s or Δ_c (see, e.g., Ref. 36). For a 2D triangular lattice, $\Delta_t = (2/\sqrt{3})^{1/2}\Delta_s$.

When working with experimental data, for a 2D lattice that is not perfect, there are two common methods of characterizing the particle spacing. First, Δ can be defined as the position of the first radial peak of the pair correlation function $g(r)$.[14] This definition is equivalent to the expression for Δ_t above in the case of an ideal triangular lattice. Most dusty plasma experimentalists use the terminology "interparticle spacing," "nearest-neighbor distance," or "average particle separation" to refer to Δ computed in this way.[10,12,13] Second, one can compute Δ_s (above) using the measured areal density. For an ideal lattice, $\Delta/\Delta_s = (2/\sqrt{3})^{1/2} \approx 1.075$, while for a real experimental lattice containing between 5% and 30% defects, we have found from our images that $\Delta/\Delta_s = 1.089$.

When computing the Coulomb coupling parameter $\Gamma = Q_0^2/b_\Gamma T \exp(-\kappa)$, the traditional choice in the theoretical literature for one-component plasmas and Yukawa plasmas is $b_\Gamma = \sqrt{1/\pi}\Delta_s$ or $b_\Gamma = \sqrt[3]{3/4\pi}\Delta_c$ for 2D and 3D, respectively.[37,38] For the purpose of comparison to theory, it is advisable to use b_Γ defined this way, as has been done in some previous plasma crystal melting experiments.[10,23] Note that $\Delta/b_\Gamma = (2\pi/\sqrt{3})^{1/2} \approx 1.90$ for an ideal 2D, triangular lattice.

APPENDIX B: DUST KINETIC TEMPERATURE MEASUREMENT

Here we discuss some important issues related to computing an accurate estimate T_{ms} to the particle kinetic temperature T using particle trajectory data obtained in plasma crystal experiments. The problems are briefly described and a solution suggested.

Equation (1) for the computed particle temperature can be rewritten as the difference between the total kinetic energy and the drift kinetic energy, $T_{ms} = m\langle v^2 \rangle - m\langle v \rangle^2$. Here, v is a single vector component of the particle velocity. Energy in correlated wave motion is included in the $m\langle v^2 \rangle$ term. We can express this explicitly by writing $m\langle v^2 \rangle = m\langle v_{th}^2 \rangle + m\langle v_{wv}^2 \rangle + m\langle v \rangle^2$, where $m\langle v_{th}^2 \rangle$ is the thermal contribution to the total kinetic energy, $m\langle v_{wv}^2 \rangle$ is that due to correlated wave motion, and $m\langle v \rangle^2$ is that due to particle drifts. In this context, $T = m\langle v_{th}^2 \rangle$. Experimentally, the difficulty lies in accurately computing $m\langle v_{wv}^2 \rangle$ and $m\langle v \rangle^2$.

In practice, it is difficult to compute the kinetic energy of coherent oscillations $m\langle v_{wv}^2 \rangle$ from experimental data. Long-wavelength compressional waves involve many particles. On

the other hand, we image only two or three particles at a time, due to the high magnification necessary to determine particle velocities accurately. Thus it is difficult to determine whether widely separated particles' motions are correlated.

The kinetic energy of drift motion $m\langle v\rangle^2$ can also be difficult to compute. The difficulty arises in how the data are sampled and averaged. If the sampling time is long compared to the time for particle drifts to change their direction, then the opposing flows are averaged together yielding $\langle v\rangle \approx 0$. In this case, the true particle drift kinetic energy is underestimated.

A possible solution to these problems is to use the relative particle velocities rather than individual particle velocities. For example, let $v_A = v_{RA} + v_{wv,A} + v_{DA}$ and $v_B = v_{RB} + v_{wv,B} + v_{DB}$, where v_R is the random part of the particle velocity, v_{wv} is that due to correlated wave motion, and v_D is that due to drift. The subscripts A and B denote two different particles appearing in the same sequence of video frames. If A and B are sufficiently close together, then $v_{wv,A} \approx v_{wv,B}$, $v_{DA} \approx v_{DB}$, and $v_{rel} = v_A - v_B \approx v_{RA} - v_{RB}$, where v_{rel} is the relative velocity. Now, $\langle v_{rel}^2 \rangle = \langle (v_{RA} - v_{RB})^2 \rangle = \langle v_{RA}^2 \rangle + \langle v_{RB}^2 \rangle - 2\langle v_{RA}\rangle\langle v_{RB}\rangle$. But $\langle v_{RA}\rangle \approx \langle v_{RB}\rangle \approx 0$, by the definition of a random velocity. Therefore, for sufficiently large averaging, $\langle v_{rel}^2 \rangle \approx 2\langle v_{RA}^2 \rangle \equiv 2\langle v_{th}^2 \rangle$ and $T_{ms} \approx 1/2\langle v_{rel}^2 \rangle$.

Unfortunately, in the present experiment we were not able to implement the relative velocity technique due to the extremely small number of particles (often just one) present in our long-distance microscope's field of view. As discussed, it is difficult in this case to account for $m\langle v_{wv}^2 \rangle$ and $m\langle v\rangle^2$ making it likely that T_{ms} overestimates T, here and in previous plasma crystal experiments.[10–12,34] While the extent of this overestimation is unknown, it is likely that the magnitudes of T_{ms} and T are strongly correlated.

APPENDIX C: ION DENSITY FLUCTUATION MEASUREMENT

Here we give a detailed explanation of the method used to measure the small amplitude ion saturation current fluctuations, which are related to δn_{rms} as discussed in Sec. III above. Two main problems required solutions. First, the small current signal had to be amplified and measured. Second, 60 Hz noise had to be minimized or accounted for to obtain a reasonable signal to noise ratio.

The normalized spectrum of ion saturation current fluctuations was obtained by computing the ratio of the ac and dc portions of the voltage drop across a 1 MΩ resistor in the external probe circuit, shown in Fig. 2(b). This ratio, expressed as a power spectrum, is identical to the saturation current spectrum $G_i(\omega) \equiv \delta I_{sat}/I_{sat}$. The ac and dc voltages were measured simultaneously using two channels of a digital oscilloscope. The average (dc) voltage drop was recorded directly on one channel of a digital oscilloscope, while the ac voltage was first filtered and amplified before being recorded on the second channel. To perform the ac measurement, each side of the 1 MΩ resistor was coupled through a very-low-frequency (0.01 Hz) high-pass filter into a unity-gain differential-input stage of the battery-powered amplifier. The signal was then passed through an active 2-pole, 10-kHz

low-pass filter and finally an X10 or X100 gain output stage. The time-averaged FFT of this signal was computed on the oscilloscope using a Hanning window, with a Nyquist frequency of 12.5 kHz, and 2.5 Hz resolution; the averaging time was ~24 s. Finally, the FFT data were normalized by the dc voltage and recorded as a single-sided power spectrum. Substantial peaks at 60 Hz and its harmonies were found in the initial ion saturation measurements.

Since only short-wavelength fluctuations were expected to heat the particles, modulations of the global plasma properties due to 60 Hz ripple in the rf generator were not expected to be physically significant. The 60 Hz modulations were verified to be global (long-wavelength) in two simple tests. In the first, light from an emission line was collected from a wide region of the plasma and measured with a photomultiplier tube. The power spectrum of this spectral emission showed distinct peaks at 60 Hz and its harmonics. In the second test, measurements of the low-frequency spectrum of the electrode voltage showed similar peaks. Since these 60 Hz fluctuations were homogenous in the plasma, they could play no role in moving one particle differently from another. Therefore they are of no interest in studying the heating of the particles.

Nevertheless, the 60 Hz noise initially proved to be so high as to obscure the desired portion of the spectrum; therefore, several steps were taken to reduce it. First, the ac-coupled amplifier described above was mounted directly on the outer end of the probe. This prevented line pickup and grounding problems present when using an external amplifier. Second, batteries were used both to bias the probe to -27 V and to power the amplifier. Third, the matching network between the rf power amplifier and the powered electrode was carefully tuned to reduce 60 Hz noise coupled to the electrode from the rf generator. For some data runs a fourth step of applying a digital filter to the measured $\delta I_{sat}/I_{sat}$ spectrum was employed. However this step was not found to alter the results significantly and it was not used for the data presented here.

[1]H. Thomas, G. E. Morfill, V. Demmel, J. Goree, B. Feuerbacher, and D. Mohlmann, Phys. Rev. Lett. **73**, 652 (1994).
[2]J. H. Chu and L. I, Phys. Rev. Lett. **72**, 4009 (1994).
[3]Y. Hayashi and K. Tachibana, Jpn. J. Appl. Phys. **33**, L804 (1994).
[4]V. E. Fortov, A. P. Nefedov, O. F. Petrov, A. A. Samarian, and A. V. Chernyschev, Phys. Rev. E **54**, R2236 (1996).
[5]V. E. Fortov, A. P. Nefedov, V. M. Torchinskiĭ, V. I. Molotkov, A. G. Krahpak, O. F. Petrov, and K. F. Volykhin, JETP Lett. **64**, 92 (1996).
[6]S. Ichimaru, Rev. Mod. Phys. **54**, 1017 (1982).
[7]D. H. E. Dubin, Phys. Rev. A **42**, 4972 (1990).
[8]In *Proceedings of the International Conference on the Physics of Strongly Coupled Plasmas*, edited by W. D. Kraeft and M. Schlanges (World Scientific, Singapore, 1996).
[9]Several variations of the interparticle separation have been used in the literature when computing Γ. This issue is discussed in Appendix A.
[10]A. Melzer, A. Homann, and A. Piel, Phys. Rev. E **53**, 2757 (1996).
[11]H. M. Thomas and G. E. Morfill, Nature (London) **379**, 806 (1996).
[12]H. M. Thomas and G. E. Morfill, J. Vac. Sci. Technol. A **14**, 501 (1996).
[13]J. B. Pieper and J. Goree, Phys. Rev. Lett. **77**, 3137 (1996).
[14]R. A. Quinn, C. Cui, J. Goree, J. B. Pieper, H. Thomas, and G. E. Morfill, Phys. Rev. E **53**, R2049 (1996).
[15]J. B. Pieper, J. Goree, and R. A. Quinn, J. Vac. Sci. Technol. A **14**, 519 (1996).
[16]C. A. Murray, in *Bond Orientational Order in Condensed Matter Systems*, edited by K. J. Strandburg (Springer-Verlag, New York, 1992), Chap 4.

[17] P. S. Epstein, Phys. Rev. **23**, 710 (1924).

[18] M. J. Baines, I. P. Williams, and A. S. Asebiomo, Mon. Not. R. Astron. Soc. **130**, 63 (1965).

[19] J. H. Chu, J.-B. Du, and L. I, J. Phys. D **27**, 296 (1994).

[20] R. A. Quinn and J. Goree, in *Physics of Dusty Plasmas, Seventh Workshop*, edited by M. Horányi, S. Robertson, and B. Walch, AIP Conf. Proc. **446** (American Institute of Physics, Woodbury, 1998), pp. 67–72.

[21] R. A. Quinn and J. Goree, Phys. Rev. E **61**, 3033 (2000).

[22] F. Melandsø and J. Goree, J. Vac. Sci. Technol. A **14**, 511 (1996).

[23] A. Melzer, V. A. Schweigert, I. V. Schweigert, A. Homann, S. Peters, and A. Piel, Phys. Rev. E **54**, R46 (1996).

[24] V. A. Schweigert, I. V. Schweigert, A. Melzer, A. Homann, and A. Piel, Phys. Rev. E **54**, 4155 (1996).

[25] C. Cui and J. Goree, IEEE Trans. Plasma Sci. **22**, 151 (1994).

[26] T. Matsoukas and M. Russell, J. Appl. Phys. **77**, 4285 (1995).

[27] T. Matsoukas, M. Russell, and M. Smith, J. Vac. Sci. Technol. A **14**, 624 (1996).

[28] O. S. Vaulina, A. P. Nefedov, O. F. Petrov, and S. A. Khrapak, JETP **88**, 1130 (1999).

[29] V. A. Godyak, R. B. Piejak, and B. M. Alexandrovich, Plasma Sources Sci. Technol. **1**, 36 (1992).

[30] E. C. Whipple, Rep. Prog. Phys. **44**, 1197 (1981).

[31] N. F. Otani and A. Bhattacharjee, Phys. Rev. Lett. **78**, 1468 (1997).

[32] F. Melandsø, Phys. Plasmas **3**, 3890 (1996).

[33] F. Melandsø, Phys. Rev. E **55**, 7495 (1997).

[34] V. V. Zhakhovskiĭ, V. I. Molotkov, A. P. Nefedov, V. M. Torchinskiĭ, A. G. Khrapak, and V. E. Fortov, JETP Lett. **66**, 419 (1997).

[35] S. Nunomura, T. Misawa, N. Ohno, and S. Takamura, Phys. Rev. Lett. **83**, 1970 (1999).

[36] F. M. Peeters and X. Wu, Phys. Rev. A **35**, 3109 (1987).

[37] I. V. Schweigert, V. A. Schweigert, V. M. Bedanov, A. Melzer, A. Homann, and A. Piel, JETP **87**, 905 (1998).

[38] S. Hamaguchi, R. T. Farouki, and D. H. E. Dubin, Phys. Rev. E **56**, 4671 (1997).